Macromolecules

pubs.acs.org/Macromolecules Article

Determination of Block Copolymer Micelle Core T_g Using ^{1}H NMR Transverse (T_2) Relaxation Measurements of Micelle Coronas

Daniel J. Fesenmeier, Hyun Chang Kim, Seyoung Kim, and You-Yeon Won*

Cite This: *Macromolecules* 2023, 56, 9156−9163 Read Online

ACCESS | Metrics & More | Article Recommendations | Supporting Information

ABSTRACT: The dynamic properties of poly(ethylene glycol) (PEG) corona chains in block copolymer (BCP) micelles were investigated with ^{1}H nuclear magnetic resonance (NMR) spectroscopy. The ^{1}H NMR spectra of BCP micelles show the PEG peak is significantly broadened, which suggests a difference in mobility in PEG segments near to the core and far from the core. ^{1}H NMR transverse (T_2) relaxation measurements suggest that the overall mobility of the PEG chains in BCP micelles is about 5−10 times slower than that of the fully hydrated PEG segments and is significantly influenced by the glass transition of the micelle core domain. The micelle core glass transition causes an increase in the Arrhenius activation energy, suggesting that the rigid nature of the core domain below T_g increases the energy barrier of rotation of the PEG near to the core domain. Therefore, this study establishes that corona T_2 measurements can be used to determine the micelle core T_g.

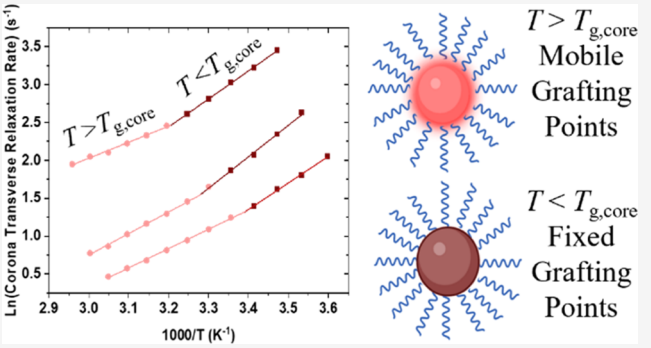

1. INTRODUCTION

With recent advances in nanomaterial technology, the question of how confinement of polymers into nanoscale dimensions impacts their glass transition properties has become one of the central questions of polymer physics. Studies over the past 20+ years have provided key insights into T_g confinement effects in polymers. For solid-supported polymer films, it has been shown that as the thickness of the film is reduced below about 100 nm, the T_g can either increase,[1,2] decrease,[3−6] or even remain unaffected,[7−9] depending on the nature of the interaction between the polymer and the substrate (solid or liquid). In free-standing film situations, the T_g of the nanoscale film is typically lower than that of the bulk polymer.[10] The glass transition behavior of self-assembled polymers at liquid interfaces (such as polymers in nanosized micelles and Langmuir films of nanoscale thickness) has been far less studied. It is not simple to think about how the micellar geometry would alter the glass transition behavior in self-assembled block copolymers (BCPs). There are several factors that need to be considered. First, the glass transition properties of polymers can be altered by the presence of solvent molecules; a plasticizing solvent nullifies the T_g nanoconfinement effect in supported polymer films.[11−13] In block polymer micelles, the block junction points are constrained to the interfacial region between the hydrophobic domain and the aqueous phase. Chemical grafting of polymer chains to a solid surface causes a significant elevation of the T_g because the chemical grafting restricts the mobility of the polymers.[14,15] In ionic liquids, the glass transition behavior of block copolymers is unaffected by micellar confinement, although micellization of block copolymers involves the restriction of the junction points to the interfacial region.[14] Nanoscale spherical confinement of homopolymers in nonsolvent media, on the other hand, produces a significant reduction of the T_g.[16,1716,17] Overall, the glass transition behavior of polymer micelles is expected to be influenced by all these factors: the nanoscale confinement, the plasticizing effect of water, and the localization of the block junction points. Therefore, it is not predictable whether a nanoscale domain formed by self-assembled block copolymers should exhibit a significantly lower T_g than that in the bulk state.

The glass transition in polymers is routinely characterized by observing discontinuous changes in thermal properties (such as specific heat) by differential scanning calorimetry (DSC). However, DSC does not provide sensitivity to a micelle glass transition in truly micellar solutions, i.e., when the polymer concentration is less than about 10%.[18] Pyrene-label intensity measurements have been shown to be able to detect micelle core T_g at less than about a few percent core content.[19−22] For

Received: July 27, 2023
Revised: October 16, 2023
Accepted: October 23, 2023
Published: November 9, 2023

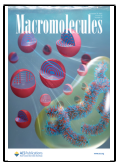

https://doi.org/10.1021/acs.macromol.3c01486
Macromolecules 2023, 56, 9156−9163

Table 1. Molecular Characteristics of BCP Micelles Post Dialysis[a]

BCP	$D_{h,DLS}$ (nm)	PDI_{DLS}	$D_{c,TEM}$ (nm)	aggregation number	interfacial area per chain (A) (nm^2)	dimensionless PEG grafting density ($\pi \cdot R_{g,PEG}^2/\alpha$)
PB(5.2 kDa)−PEG(4.5 kDa)	42.6 ± 0.2	0.16 ± 0.01	19.5[37]	404	2.95	6.6
PtBMA(6.5 kDa)−PEG(5.0 kDa)	25.4 ± 0.2	0.14 ± 0.02	17.1 ± 1.2	215	3.66	5.8
PS(1.6 kDa)−PEG(5.0 kDa)	21.4 ± 0.1	0.15 ± 0.01	13.7 ± 0.8	545	1.08	19.6
PS(5.2 kDa)−PEG(5.5 kDa)	28.6 ± 0.2	0.11 ± 0.02	18.4 ± 0.7	396	2.68	8.5
PS(13.8 kDa)−PEG(5.0 kDa)	52.9 ± 0.8	0.07 ± 0.02	42.8 ± 2.2	2359	3.07	6.9

[a]The hydrodynamic diameter (D_h) and polydispersity index (PDI) were measured from DLS, and the core diameter (D_c) was measured using TEM. The errors for D_h and PDI are standard deviations from 5 measurements; the errors for D_c are standard deviations from 10 separate particles. For PB−PEG, the core diameter value was estimated from a previous study for which TEM was done after cross-linking PB core domains, which prevented aggregation during the drying process.[37,38] To calculate the aggregation number, the density of the core domain in the bulk was used. $R_{g,PEG}$ is the radius of gyration of the PEG block in the 3D self-avoiding random walk configuration (≅2.6 nm for PEG(5.0 kDa) and 2.7 nm for PEG(5.5 kDa)).

use in aqueous solutions, pyrene must be chemically conjugated to the polymer because pyrene is soluble in water to some extent. Techniques that have proven to be useful for measuring T_g in Langmuir polymer films, such as surface thermodynamic analysis,[23] surface nonlinear stress relaxation measurement,[24] and surface linear dynamic mechanical spectroscopy,[25] cannot be employed in micellar situations due to the absence of a sample-spanning macroscopic dimension in the micelle geometry.

In the present study, it is demonstrated for the first time that the micelle core T_g can be directly determined in an aqueous block copolymer solution by proton NMR transverse (T_2) relaxation measurements. Previously, NMR T_2 relaxation techniques have been shown to be useful for determination of the glass transition in polymer electrolytes[26] and biopolymer (sugar) solutions[27] and also for the measurement of the dynamic properties of corona chains in micelles formed by nonionic surfactants[28,29] and block copolymers.[30−32] However, to the best of our knowledge, the feasibility of using the micelle corona NMR transverse relaxation for the determination of the micelle core T_g has not previously been demonstrated. The NMR study provides a new alternative to other available micelle core T_g measurement techniques.

2. EXPERIMENTAL SECTION

2.1. Materials. PS(5.2 kDa)−PEG(5.5 kDa) and 1,2-PB(5.2 kDa)−PEG(4.5 kDa) were purchased from Polymer Source, Inc. and were synthesized using living anionic polymerization. PS(1.6 kDa)−PEG(5.0 kDa), PS(13.8 kDa)−PEG(5.0 kDa), and PtBMA(6.5 kDa)−PEG(5.0 kDa) were synthesized using reversible addition−fragmentation chain transfer (RAFT) polymerization as previously described in detail.[33] Briefly, PEG(5.0 kDa) (Sigma) was conjugated to the RAFT agent, 4-cyano-4-[(dodecylsulfanylthiocarbonyl)-sulfanyl]pentanoic acid (CDSP), followed by subsequent PS/PtBMA polymerization.

2.2. Polymer Characterization. The number-average molecular weight of the RAFT synthesized polymers was determined by ^{1}H NMR using a Bruker Avance III 800 MHz spectrometer. The measurements were done in deuterated chloroform at a concentration of 5 wt %. The polydispersity indices were determined using gel permeation chromatography (GPC) using a Waters 1515 isocratic pump equipped with Styragel HR 4 and Ultrastyragel columns. The mobile phase was THF, and the flow rate was 1 mL/min. Calibration was done using polystyrene standards.

2.3. Micelle Formulation. Equilibration-nanoprecipitation (ENP) was used to formulate micelles.[34] Briefly, 50 mg of the block copolymers was added to 5 mL of a water/acetone mixture and stirred vigorously overnight using a magnetic stirrer. For all polymers except the PS(13.8 kDa)−PEG(5.0 kDa), an initial solvent composition of 30% water/70% acetone was used. For PS(13.8 kDa)−PEG(5 kDa), an initial solvent composition of 5% water/95% acetone was used. After equilibration, the acetone was removed by dialysis against 4 L of Milli-Q water using 50 kDa MWCO dialysis tubing, replacing the water twice over a 24-h period.

2.4. Dynamic Light Scattering (DLS). The hydrodynamic diameters of the block copolymer micelles were measured at 25 °C by DLS using a Brookhaven ZetaPALS instrument. The scattering intensities were measured by using a 659 nm laser at a scattering angle of 90°. The hydrodynamic diameters were calculated from the measured diffusion coefficients by using the Stokes−Einstein equation. For DLS measurements, the samples were diluted to guarantee single scattering and filtered with 0.45 μm syringe filters to remove contaminants.

2.5. Transmission Electron Microscopy (TEM). TEM specimens were prepared by placing 20 μL of a 0.01−0.05 mg/mL polymer micelle solution on a carbon-coated copper TEM grid (treated using an O_2 plasma cleaner to make the surface more hydrophilic). A total of 10 μL of a 2% uranyl acetate solution was added to the sample solution already placed on the TEM grid, and the mixture was blotted by using filter paper and dried. The samples thus prepared were imaged using a 200 kV FEI Tecnai 20 TEM instrument. The TEM images were analyzed by using ImageJ software.

2.6. T_2 (spin−spin) ^{1}H NMR Relaxation Measurement of Polymer Micelles. Samples were prepared in deuterated water (D_2O) by using 10 kDa Amicon centrifuge membranes to perform a series of concentration and dilution steps to switch the solvent from H_2O to D_2O until the final H_2O content was less than 0.1% by volume. The final concentration of polymer micelles in D_2O was 3.5 mg/mL. The NMR measurements were carried out on a Bruker Advance III 800 MHz spectrometer operating with Bruker Topspin 3.2 software. A self-compensating Carr−Purcell−Meiboom−Gill (CPMG) echo sequence ("$90_x - \tau - (180_y - 2\tau)_n$") was used for the T_2 relaxation measurements.[35,36] The parameters used for obtaining the data were: τ = 500 μs; n = 1, 5, 15, 40, 80, 250, 600, and 900; number of scans per free induction decay = 16; delay time between recycles = 4 s. The intensity of the echo was measured at the following times: t = 1.015, 2.030, 4.061, 5.076, 8.122, 16.24, 32.49, 64.97, 81.22, 129.9, 259.9, 519.8, 710.6, 1.040 × 10^3, 1.523 × 10^3, and 2.079 × 10^3 μs. The 90° pulse was calibrated for each sample at each temperature. The measurements were carried out at various temperatures with 5 K intervals during heating from 283 to 343 K. At each measurement temperature, the sample was equilibrated for 10 min prior to the measurement followed by shimming (Topshim) and probe tuning (ATMA) routines. The raw intensity vs time data was obtained using MestreNova software by analyzing stacked spectra containing the spectra from each time point and using the integral graph function over the entire PEG proton peak. The fits of the relaxation profiles were made using OriginPro software.

2.7. Preparation and Measurement of the Fluorescence Intensities of FCVJ-Loaded BCP Micelles in Water. Farnesyl-(2-carboxy-2-cyanovinyl)-4 julolidine (FCVJ) was loaded in micelles by using Flash Nanoprecipitation (FNP). For FNP, a microfluidic chip (NanoFabTx microfluidic mixer (Sigma-Aldrich)) was used to rapidly

https://doi.org/10.1021/acs.macromol.3c01486
Macromolecules 2023, 56, 9156−9163

mix an organic stream consisting of acetone, BCP, and FCVJ with water. The BCP concentration in the organic stream was 12 mg/mL, and the BCP to FCVJ mass ratio was 1:1000. The ratio of the water volume flow rate to the organic stream volume flow rate was 11:1. After mixing, the remaining acetone was removed by centrifugal dialysis using an Amicon Ultra-15 filter unit to a final concentration of 5 mg/mL. The fluorescence intensities were measured using an Agilent Technology Cary Eclipse fluorescence spectrophotometer. The temperature was controlled by using a Peltier temperature control system. The excitation/emission wavelengths were used, which gave the maximum fluorescence intensity. The sample was calibrated at each temperature for 5 min prior to measurement.

3. RESULTS AND DISCUSSION

Five different poly(ethylene glycol) (PEG)-based block copolymers (BCPs) were formulated for the T_2 NMR study. The hydrophobic block core chemistries used were polystyrene (PS), poly(*tert*-butyl methacrylate) (PtBMA), and poly-(1,2(95%)-butadiene) (PB) with molecular weights of PS(13.8 kDa)−PEG(5.0 kDa), PS(5.2 kDa)−PEG(5.5 kDa), PS(1.6 kDa)−PEG(5.0 kDa), PtBMA(6.5 kDa)−PEG(5.0 kDa), and PB(5.2 kDa)−PEG(4.5 kDa). Micelles were formulated using equilibration-nanoprecipitation (ENP)[34] at an initial volume percentage of 30% water/70% acetone for all BCPs except PS(13.8 kDa)−PEG(5.0 kDa) for which a 5% water/95% acetone composition was used. The size characteristics of the BCP micelles after the removal of acetone are shown in Table 1. TEM images are shown in Figure S1.

Standard ^{1}H NMR was taken at 25 °C for each micelle system and for the 5.0 kDa PEG homopolymer in D_2O. The PEG peaks are compared for each system in Figure 1. The

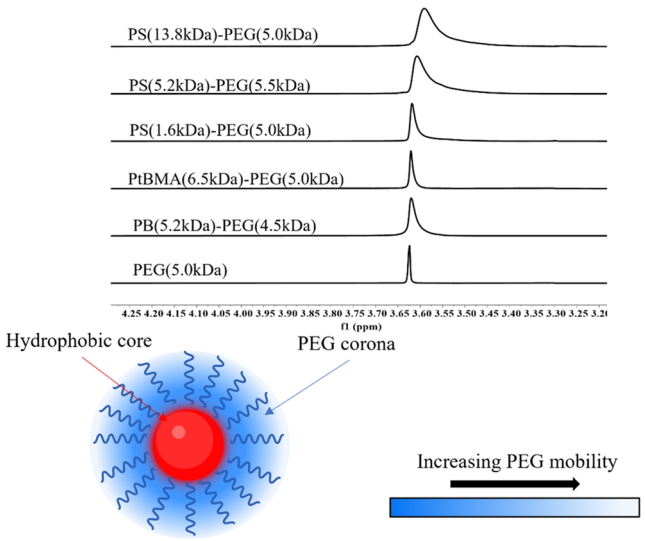

Figure 1. (Top) ^{1}H NMR spectrum of PEG protons of BCP micelles and the PEG homopolymer in D_2O at 25 °C. (Bottom) Schematic of the BCP micelle structure and origin of PEG ^{1}H NMR peak broadening.

PEG peak is clearly broadened in the micelle systems compared to the PEG homopolymer peak. This broadening has been reported previously for PEG−PLA micelle systems and suggests a disparity in the mobility of PEG $-CH_2-$ segments near the core domain and far from the core domain.[39] The segments near the core domain are expected to have reduced mobility due to the proximity to the core junction point and the higher concentration of PEG near the core.[40]

The results suggest that the degree of broadening of the PEG's $-CH_2-$ peak is influenced by both the molecular weight and the chemistry of the core block. For the three PS−PEG systems, the PEG peak becomes broader as the molecular weight of the PS block is increased, which suggests a greater disparity in mobility between segments near the block junction point and those far from the junction point. Given that the T_g of polymers increases with increasing molecular weight, the higher molecular weight PS domains are expected to be more rigid at a given temperature, which further reduces the mobility of PEG segments near the core domain. In addition to the effect of core block molecular weight, the chemistry of the core block appears to also play a role as the PtBMA(6.4 kDa)−PEG(5.0 kDa) micelles, which have similar size and M_n properties to the PS(5.2 kDa)−PEG(5.5 kDa) micelles, have a much sharper PEG peak. This is likely influenced by the interfacial tension of the core block with water, as PtBMA has a relatively lower water interfacial tension value (13 mN/m) compared to PS (28 mN/m). The lower interfacial tension with water suggests a lesser change in the hydration state of PEG chains near the core domain.

To analyze the effect of temperature on the mobility of PEG chains, T_2 ^{1}H NMR measurements of PEG protons were taken at 5 K intervals. For PEG(5.0 kDa) homopolymer in D_2O, the relaxation profile fits well to a monoexponential decay function in the form of $G(t) = A \exp(-R_2 t)$, where R_2 is the transverse relaxation rate defined as $1/T_2$. However, for the micelle systems, the PEG relaxation did not follow the monoexponential decay, which is not surprising given the previous discussion regarding the broadening of the PEG peak. Therefore, for the micelle cases, a stretched exponential model was used to fit the relaxation profiles in the form of $G(t) = A \exp[-(R_2 t)^{\beta}]$. The stretched exponential function has been used previously to describe systems with a continuous spectrum of relaxation times and thus is a reasonable choice for the PEG corona scenario.[41]

The results for the R_2 relaxation rates as a function of the temperature along with Arrhenius plots of the relaxation rates are shown in Figure 2. The relaxation decay profiles ($G(t)$) and their corresponding fits are shown in Figure S2. The results show that for all cases, R_2 decreases with increasing temperature, which is consistent with an increase in motion of the PEG segments at higher temperatures. The magnitude of R_2 at a given temperature is increased by over an order of magnitude in the micelle cases compared to the PEG homopolymer case, indicating a decrease in overall PEG mobility. For the three PS−PEG micelle systems, the magnitude of R_2 increases with the increasing molecular weight of the PS block. The increase in R_2 for higher M_n PS core domains corresponds well with the increased broadening of the PEG peak. These results both suggest that increasing the M_n of the core PS block causes a significant decrease in the mobility of the PEG chains near the core domain, which causes an increase in the width of the PEG peak and the overall R_2 values. The core chemistry also appears to have an effect such that when comparing the three systems with similar core molecular weights, PtBMA(6.5 kDa)−PEG(5.0 kDa), PS(5.2 kDa)−PEG(5.5 kDa), and PB(5.2 kDa)−PEG(4.5 kDa), there is an increase in the overall R_2 with increasing core interfacial tension with water where $\gamma_{PtBMA\text{-}water}$ = 25 mN/m,[37,42] $\gamma_{PS\text{-}water}$ = 39 mN/m,[37,42] and $\gamma_{PB\text{-}water}$ = 51 mN/m.[43,44] The polymer−

https://doi.org/10.1021/acs.macromol.3c01486
Macromolecules 2023, 56, 9156−9163

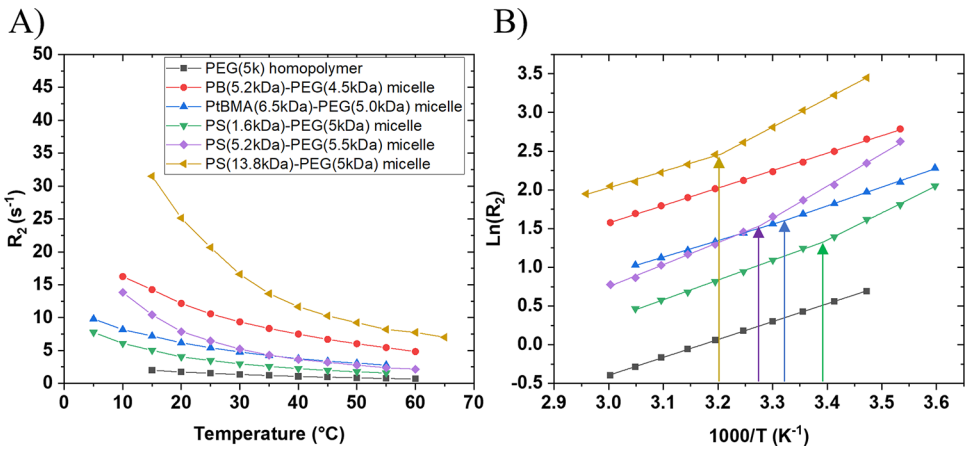

Figure 2. (A) Transverse relaxation rates ($R_2 = 1/T_2$) of PEG protons of BCP micelles and of PEG homopolymer in D_2O, and (B) Arrhenius plots of relaxation rates along with arrows indicating core T_g where applicable.

Table 2. Average β Values from the Stretched Exponential Fits of the Transverse Relaxation Profiles, the Arrhenius Activation Energy Constants (E_a) Above and Below Core T_g (where applicable) Calculated from Slope of Arrhenius Plots, the Core $T_{g,NMR}$ Calculated from Piecewise Linear Fits of Arrhenius Plots, and the Core $T_{g,FCVJ}$ Ranges for Two Micelles of the Samples[a]

BCP	β_{avg}	$E_{a,\,T>T_g}$ (J/mol)	$E_{a,\,T<T_g}$ (J/mol)	core $T_{g,NMR}$ (°C)	core $T_{g,min,FCVJ}$ (°C)	core $T_{g,mean,FCVJ}$ (°C)	core $T_{g,max,FCVJ}$ (°C)
PEG(5.0 kDa)	N/A	19.2	N/A	N/A			
PB(5.2 kDa)−PEG(5.0 kDa)	0.75 ± 0.03	18.7	N/A	N/A			
PtBMA(6.5 kDa)−PEG(5.0 kDa)	0.72 ± 0.02	17.6	20.2	28.1 ± 2.1	22	33	44
PS(1.6 kDa)−PEG(5.0 kDa)	0.78 ± 0.03	21.2	29.2	21.8 ± 1.2			
PS(5.2 kDa)−PEG(5.5 kDa)	0.75 ± 0.03	23.6	34.6	32.1 ± 1.4	17	41	65
PS(13.8 kDa)−PEG(5.0 kDa)	0.70 ± 0.02	17.6	30.8	38.8 ± 1.1			

[a]The error of the β_{avg} values is the standard deviation of the best-fit β values at each temperature. The error for $T_{g,NMR}$ is the 95% confidence interval based on the piecewise linear fit to the Arrhenius plots of each sample. The confidence intervals of the derived parameters are calculated in OriginPro software using the Asymptotic-Symmetry Method.

water interfacial tension values were estimated from Young's equation using literature values for polymer−water contact angle and polymer−air surface tension, and the values are shown in Table S1.

The Arrhenius plots in Figure 2B demonstrate interesting differences in the effect of the temperature on R_2 values. For the PEG homopolymer, R_2 displays clear Arrhenius behavior indicated by the linear relationship between $\ln(R_2)$ and temperature over the entire temperature range. Despite having much higher R_2 values, PB−PEG follows Arrhenius behavior ($R_2 \sim \exp(E_a/(RT))$ where R is the gas constant) over the entire temperature range, which indicates no transition in the energy barriers for relaxation. However, for the PS−PEG and PtBMA-PEG cases, there is an evident discontinuity in the Arrhenius behavior such that the Arrhenius plots cannot be described well by a single E_a constant over the entire temperature range. Instead, there is an increase in the slope at low temperatures. The origin of this transition point is proposed to be due to the glass transition of the outer layer of the core domain. The temperature of this transition point was estimated using a piecewise linear fit of the Arrhenius plots and is shown in Table 2 along with corresponding E_a values, which were calculated from the slopes. Also, a comparison of R_2 values and Arrhenius fits from a heating and cooling cycle for one PS−PEG micelle sample are shown in Figure S3 and Table S2, which demonstrates the reproducibility of the NMR measurements.

The proposed mechanism of the effect of core T_g on R_2 is as follows. When the outer layer of the core domain is above the core T_g, the block junction point can freely move within the core matrix. When the outer layer of the core domain is below the core T_g, the mobility of the block junction point is greatly reduced. The changing of the environment of the grafting junction from mobile to immobile creates an increase in the energy barrier of rotation for the PEG chains near the core domain, which results in an increase in the slope in the R_2 Arrhenius plots for $T < T_g$. It should be emphasized that the measured T_g is proposed to be the T_g of the outer layer of the PS core and that this will likely be less than that of the internal core T_g as previous reports have shown that there exists in gradient in T_g values for nanoconfined PS domains.[1]

Given the mechanism of the detection of core T_g using T_2 NMR, it is expected that increasing the percentage of corona segments near the core will increase the magnitude of change in the Arrhenius E_a values. Therefore, micelles with lower corona grafting densities are expected to show a larger increase in the slope below T_g, and this is indeed reflected in the PS−PEG samples. A similar effect would be expected if, for example, the molecular weight of the corona block was decreased or the corona chemistry was modified to be more hydrophobic.[45]

The measured core T_g values demonstrate a significant reduction in core T_g compared to that of the bulk material. Figure 3 shows a comparison of the core T_g of the PS domains and of the bulk T_g values using the Flory−Fox equation.[46] The

https://doi.org/10.1021/acs.macromol.3c01486
Macromolecules 2023, 56, 9156−9163

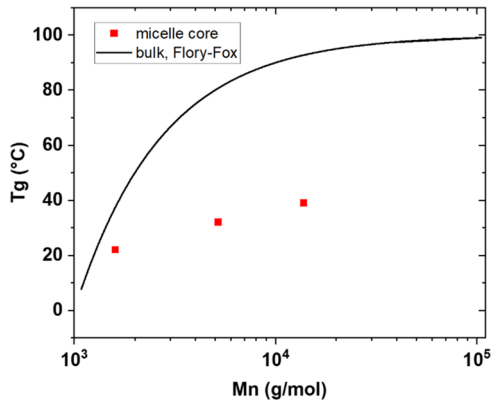

Figure 3. Comparison of the PS core T_g measured from ^{1}H NMR to the values of the bulk T_g predicted by using the Flory−Fox equation ($T_g = T_{g,\infty} - K/M_n$, where $T_{g,\infty}$ = 100 °C and $K = 1 \times 10^5$ g/mol for PS).

magnitude of T_g reduction is the least for the PS(1.6 kDa)−PEG(5.0 kDa) micelles, which have the smallest diameter, whereas a previous study showed T_g depression for PS nanospheres increases with decreasing diameter below 100 nm.[16] The same study also revealed that adding a nonionic surfactant to PS nanospheres limited the T_g depression due to reduction of free volume in the mobile outer PS layer by the inclusion of the nonionic surfactant molecules.[16] Therefore, the extremely high density of PEG chains that occurs in the lower molecular weight PS(1.5 kDa)−PEG(5.0 kDa) micelle case may also cause a reduction in the free volume of the outer PS layer. The relatively lower interfacial tension with water of PtBMA likely increases the reduction of T_g compared to PS due to the more favorable interactions of PtBMA and water.

Last, to corroborate the values obtained from the T_2 NMR technique, an alternative analysis of the core T_g was done using a fluorescent molecular rotor technique, which has recently been shown to be the robust method to measure the T_g of polymer materials.[47] The fluorescent molecular rotor, farnesyl-(2-carboxy-2-cyanovinyl)-julolidine (FCVJ), was encapsulated in the core domain of PS(5.2 kDa)−PEG(5.5 kDa) and PtBMA(6.5 kDa)−PEG(5.0 kDa) micelles. The fluorescent intensities of the encapsulated FCVJ were measured as a function of the temperature, and the results are shown in Figure 4. Upon excitation, the FCVJ rotor can either rotate or fluoresce such that, as the local viscosity decreases, the fluorescence intensity decreases. Furthermore, the fluorescence intensity (I) can be related to changes in the free volume of the core domain using the Loutfy-Locally Correlated Lattice (LCL) model, which predicts a discontinuity in log(I) vs temperature at T_g. For the case when FCVJ is encapsulated in a micelle core, it has been shown that the log(I) vs temperature (T) data cannot be modeled well by a single T_g (due to random radial distribution of FCVJ molecules). However, convolution of the Loutfy-LCL model with a simple flat T_g distribution produces a sufficient model fit and thus is applied in this study. A detailed description of the fitting procedure is provided in Supporting Information. The core $T_{g,min}$, $T_{g,mean}$, $T_{g,max}$ derived from the model fits of log(I) vs T data were 17,

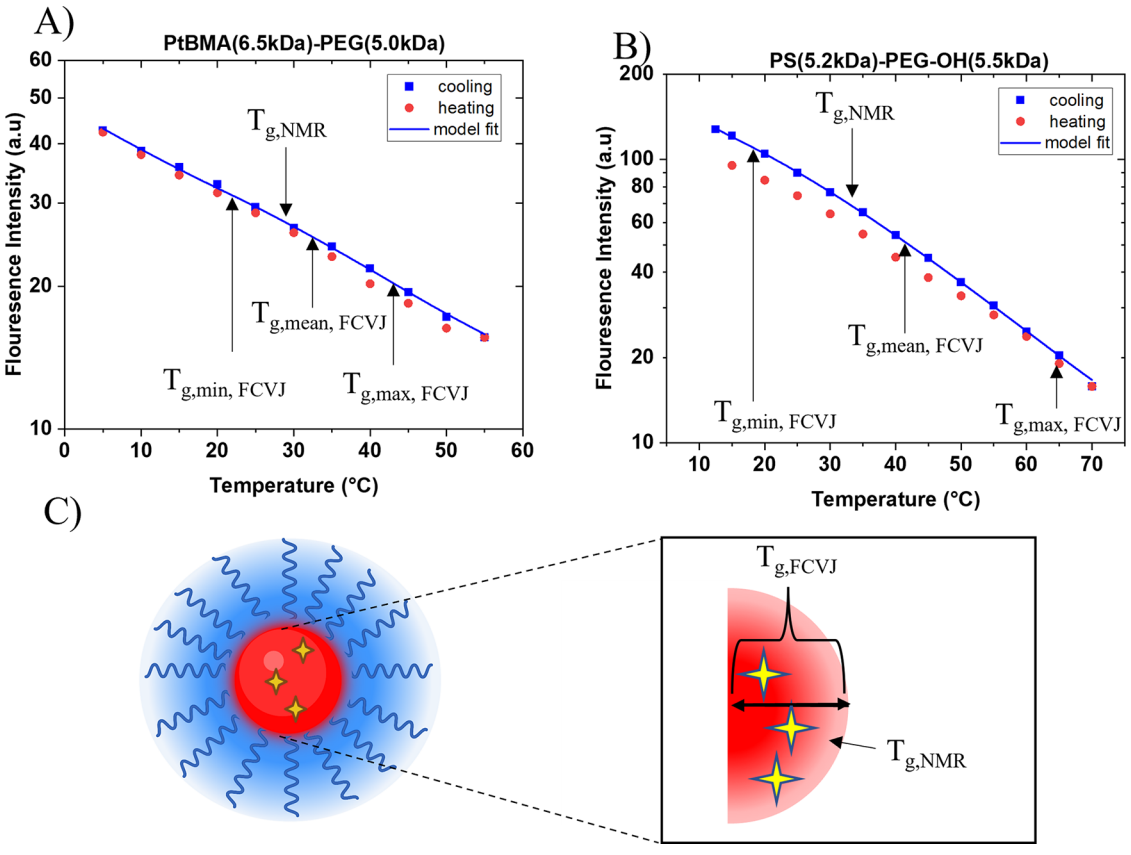

Figure 4. Fluorescence intensity log(I) vs temperature (T) plots of FCVJ-loaded (A) PtBMA(6.5 kDa)−PEG(5.0 kDa) and (B) PS(5.2 kDa)−PEG(5.5 kDa) micelles for heating and cooling cycles along with model fits to determine core $T_{g,min,FCVJ}$, $T_{g,mean,FCVJ}$, $T_{g,max,FCVJ}$. (C) Schematic illustration of differences between core T_g determined by using FCVJ and T_2 NMR.

https://doi.org/10.1021/acs.macromol.3c01486
Macromolecules 2023, 56, 9156−9163

41, and 65 °C for PS(5.2 kDa)−PEG(5.5 kDa) and 22, 33, and 44 °C for PtBMA(6.5 kDa)−PEG(5.0 kDa). For both cases, the T_g from T_2 NMR falls between $T_{g,min}$ and $T_{g,mean}$, from FCVJ. Since the core T_g is expected to increase with distance away from the water interface, the T_g range between $T_{g,min}$ and $T_{g,mean}$ represents the outer region of the micelle core; therefore, the T_g from T_2 NMR falling within this range provides further validation for the technique.

Although there is good qualitative agreement between the FCVJ and NMR techniques, there is a discrepancy between the T_g range obtained from FCVJ measurements and the values from NMR. The model used for the analysis of the fluorescent intensity−temperature data requires an imputed T_g distribution to account for the spatial distribution of the rotor within the core. For simplicity, the fitting results obtained in this manuscript were completed using a nonweighted distribution ranging from $T_{g,min}$ to $T_{g,max}$. Therefore, the results for the T_g range from the FCVJ method only provide a rough estimation of the range of T_g values within the core and cannot be expected to be as accurate as the values obtained from NMR. In order to obtain a rigorous comparison between the two methods, the exact spatial distribution of the FCVJ compound in the core would need to be obtained, using small-angle neutron scattering (SANS), for example, which could then be input into the FCVJ model to obtain a precise fit of the FCVP temperature-intensity data. Additionally, the size of the micelles used in the two studies varied slightly because an alternative formulation method had to be used to encapsulate the hydrophobic FCVJ compound in the micelle cores. The core diameters of PS(5.2 kDa)−PEG(5.5 kDa) and PtBMA-(6.5 kDa)−PEG(5.0 kDa) micelles in NMR measurements were 18.4 and 17.1 nm, respectively, while for FCVJ, the core diameters were 14.0 and 17.5 nm, respectively. The TEM images for the FCVJ samples are shown in Figure S4. Therefore, differences in size and the unknown spatial distribution of FCVJ in the core both contribute to the slight discrepancy between the two methods.

4. CONCLUSIONS

A novel technique using T_2 ^{1}H NMR of micelle corona chains to determine micelle core T_g has been successfully demonstrated. Specifically, this technique measures the T_g of the outer region of the micelle core by measuring changes in the Arrhenius behavior of the transverse relaxation rate of micelle corona (PEG in this study) protons. This technique is done using low concentrations (3 mg/mL) of pristine micelles in D_2O. The results demonstrate the T_g of the outer core region is significantly suppressed compared to the bulk T_g values, and the magnitude of the suppression is affected by the molecular weight and chemistry of the core block.

■ ASSOCIATED CONTENT

Supporting Information

The Supporting Information is available free of charge at https://pubs.acs.org/doi/10.1021/acs.macromol.3c01486.

Contains detailed description of fitting procedure for FCVJ analysis and supplementary figures of TEM images of samples used in NMR (Figure S1), transverse relaxation profiles ($G(t)$), and corresponding fits at each temperature (Figure S2); heating and cooling data transverse relaxation results for PS(5.2 kDa)-PEG(5.5 kDa) (Figure S3 and Table S2); TEM images for FCVJ samples (Figure S4); and water contact angle and surface tension values for the hydrophobic blocks used in this study (Table S1) (PDF)

■ AUTHOR INFORMATION

Corresponding Author

You-Yeon Won − *Davidson School of Chemical Engineering, Purdue University, West Lafayette, Indiana 47907, United States; Institute of Cancer Research, Purdue University, West Lafayette, Indiana 47907, United States;* orcid.org/0000-0002-8347-6375; Email: yywon@purdue.edu

Authors

Daniel J. Fesenmeier − *Davidson School of Chemical Engineering, Purdue University, West Lafayette, Indiana 47907, United States*

Hyun Chang Kim − *Davidson School of Chemical Engineering, Purdue University, West Lafayette, Indiana 47907, United States*

Seyoung Kim − *Davidson School of Chemical Engineering, Purdue University, West Lafayette, Indiana 47907, United States; Department of Polymer Science and Engineering, Dankook University, Yongin, Gyeonggi 16890, Republic of Korea*

Complete contact information is available at: https://pubs.acs.org/10.1021/acs.macromol.3c01486

Notes

The authors declare no competing financial interest.

■ ACKNOWLEDGMENTS

The authors are grateful for funding from ACS PRF (60233-ND7) and NSF (CBET-2211843). The authors also acknowledge support from the Purdue University Institute for Cancer Research (PCCR) via an NIH NCI grant (P30 CA023168), which supports the campus-wide NMR shared resources that were utilized in this work.

■ REFERENCES

(1) Ellison, C. J.; Torkelson, J. M. The distribution of glass-transition temperatures in nanoscopically confined glass formers. *Nat. Mater.* **2003**, *2* (10), 695−700.

(2) Fryer, D. S.; Peters, R. D.; Kim, E. J.; Tomaszewski, J. E.; de Pablo, J. J.; Nealey, P. F.; White, C. C.; Wu, W.-l. Dependence of the Glass Transition Temperature of Polymer Films on Interfacial Energy and Thickness. *Macromolecules* **2001**, *34* (16), 5627−5634.

(3) Keddie, J. L.; Jones, R. A. L.; Cory, R. A. Size-Dependent Depression of the Glass Transition Temperature in Polymer Films. *Europhys. Lett.* **1994**, *27* (1), 59.

(4) Tsui, O. K. C.; Russell, T. P.; Hawker, C. J. Effect of interfacial interactions on the glass transition of polymer thin films. *Macromolecules* **2001**, *34* (16), 5535−5539.

(5) Bodiguel, H.; Fretigny, C. Viscoelastic properties of ultrathin polystyrene films. *Macromolecules* **2007**, *40* (20), 7291−7298.

(6) Wang, J.; McKenna, G. B. Viscoelastic and glass transition properties of ultrathin polystyrene films by dewetting from liquid glycerol. *Macromolecules* **2013**, *46* (6), 2485−2495.

(7) O'Connell, P. A.; Hutcheson, S. A.; McKenna, G. B. Creep behavior of ultra-thin polymer films. *J. Polym. Sci., Part B: Polym. Phys.* **2008**, *46* (18), 1952−1965.

(8) O'Connell, P. A.; McKenna, G. Rheological measurements of the thermoviscoelastic response of ultrathin polymer films. *Science* **2005**, *307* (5716), 1760−1763.

(9) Spièce, J.; Martínez-Tong, D. E.; Sferrazza, M.; Nogales, A.; Napolitano, S. Are polymers glassier upon confinement? *Soft Matter* **2015**, *11* (31), 6179−6186.
(10) Forrest, J. A.; Dalnoki-Veress, K.; Dutcher, J. Interface and chain confinement effects on the glass transition temperature of thin polymer films. *Phys. Rev. E* **1997**, *56* (5), 5705.
(11) Ellison, C. J.; Ruszkowski, R. L.; Fredin, N. J.; Torkelson, J. M. Dramatic reduction of the effect of nanoconfinement on the glass transition of polymer films via addition of small-molecule diluent. *Phys. Rev. Lett.* **2004**, *92* (9), No. 095702.
(12) Kim, S.; Mundra, M. K.; Roth, C. B.; Torkelson, J. M. Suppression of the T g-nanoconfinement effect in thin poly (vinyl acetate) films by sorbed water. *Macromolecules* **2010**, *43* (11), 5158−5161.
(13) Riggleman, R. A.; Douglas, J. F.; de Pablo, J. J. Tuning polymer melt fragility with antiplasticizer additives. *J. Chem. Phys.* **2007**, *126* (23), No. 234903.
(14) Yamamoto, S.; Tsujii, Y.; Fukuda, T. Glass transition temperatures of high-density poly (methyl methacrylate) brushes. *Macromolecules* **2002**, *35* (16), 6077−6079.
(15) Tate, R. S.; Fryer, D. S.; Pasqualini, S.; Montague, M. F.; de Pablo, J. J.; Nealey, P. F. Extraordinary elevation of the glass transition temperature of thin polymer films grafted to silicon oxide substrates. *J. Chem. Phys.* **2001**, *115* (21), 9982−9990.
(16) Feng, S.; Li, Z.; Liu, R.; Mai, B.; Wu, Q.; Liang, G.; Gao, H.; Zhu, F. Glass transition of polystyrene nanospheres under different confined environments in aqueous dispersions. *Soft Matter* **2013**, *9* (18), 4614−4620.
(17) Zhang, C.; Guo, Y.; Priestley, R. D. Glass transition temperature of polymer nanoparticles under soft and hard confinement. *Macromolecules* **2011**, *44* (10), 4001−4006.
(18) Evans, C. M.; Deng, H.; Jager, W. F.; Torkelson, J. M. Fragility is a key parameter in determining the magnitude of T g-confinement effects in polymer films. *Macromolecules* **2013**, *46* (15), 6091−6103.
(19) Evans, C. M.; Henderson, K. J.; Saathoff, J. D.; Shull, K. R.; Torkelson, J. M. Simultaneous determination of critical micelle temperature and micelle core glass transition temperature of block copolymer−solvent systems via pyrene-label fluorescence. *Macromolecules* **2013**, *46* (10), 4131−4140.
(20) Jule, E.; Yamamoto, Y.; Thouvenin, M.; Nagasaki, Y.; Kataoka, K. Thermal characterization of poly (ethylene glycol)−poly (d, l-lactide) block copolymer micelles based on pyrene excimer formation. *J. Controlled Release* **2004**, *97* (3), 407−419, DOI: 10.1016/j.jconrel.2004.02.012.
(21) Mok, M. M.; Lodge, T. P. Temperature-based fluorescence measurements of pyrene in block copolymer micelles: Probing micelle core glass transition breadths. *J. Polym. Sci., Part B: Polym. Phys.* **2012**, *50* (7), 500−515.
(22) Wei, W.-C.; Feng, S.; Zheng, C.-X.; Liang, G.-D.; Gao, H.-Y.; Wu, Q.; Zhu, F.-M. Glass transition and quantum yield for fluorescent labelled polystyrene core-forming block in self-assembled nanomicelles of amphiphilic diblock copolymers. *J. Polym. Res.* **2015**, *22*, 212.
(23) Kim, H. C.; Arick, D. Q.; Won, Y. Y. Air-Water Interfacial Properties of Chloroform-Spread versus Water-Spread Poly((D,L-lactic acid-co-glycolic acid)-block-ethylene glycol) (PLGA-PEG) Polymers. *Langmuir* **2018**, *34* (16), 4874−4887.
(24) Kim, H. C.; Lee, H.; Khetan, J.; Won, Y. Y. Surface Mechanical and Rheological Behaviors of Biocompatible Poly((D,L-lactic acid-ran-glycolic acid)-block-ethylene glycol) (PLGA-PEG) and Poly((D,L-lactic acid-ran-glycolic acid-ran-epsilon-caprolactone)-block-ethylene glycol) (PLGACL-PEG) Block Copolymers at the Air-Water Interface. *Langmuir* **2015**, *31* (51), 13821−13833.
(25) Kim, H. C.; Lee, H.; Jung, H.; Choi, Y. H.; Meron, M.; Lin, B. H.; Bang, J.; Won, Y. Y. Humidity-dependent compression-induced glass transition of the air-water interfacial Langmuir films of poly(D,L-lactic acid-ran-glycolic acid) (PLGA). *Soft Matter* **2015**, *11* (28), 5666−5677.
(26) Ries, M. E.; Klein, P.; Brereton, M.; Ward, I. Proton NMR study of rouse dynamics and ideal glass transition temperature of poly (ethylene oxide) LiCF3SO3 complexes. *Macromolecules* **1998**, *31* (15), 4950−4956.
(27) Hills, B.; Pardoe, K. Proton and deuterium NMR studies of the glass transition in a 10% water-maltose solution. *J. Mol. Liq.* **1995**, *63* (3), 229−237.
(28) Ferreira, T. M.; Bernin, D.; Topgaard, D. NMR studies of nonionic surfactants. *Annu. Rep. NMR Spectrosc.* **2013**, *79*, 73−127.
(29) Carlström, G.; Halle, B. The state of water in non-ionic surfactant solutions and lyotropic phases. Oxygen-17 magnetic relaxation study. *J. Chem. Soc., Faraday Trans. 1* **1989**, *85* (5), 1049−1063.
(30) Weiss, J.; Wienk, H.; Boelens, R.; Laschewsky, A. Block Copolymer Micelles with an Intermediate Star-/Flower-Like Structure Studied by 1H NMR Relaxometry. *Macromol. Chem. Phys.* **2014**, *215* (9), 915−919.
(31) de Graaf, A. J.; Boere, K. W.; Kemmink, J.; Fokkink, R. G.; van Nostrum, C. F.; Rijkers, D. T.; van der Gucht, J.; Wienk, H.; Baldus, M.; Mastrobattista, E.; et al. Looped structure of flowerlike micelles revealed by 1H NMR relaxometry and light scattering. *Langmuir* **2011**, *27* (16), 9843−9848.
(32) Wada, H.; Kitazawa, Y.; Kuroki, S.; Tezuka, Y.; Yamamoto, T. NMR relaxometry for the thermal stability and phase transition mechanism of flower-like micelles from linear and cyclic amphiphilic block copolymers. *Langmuir* **2015**, *31* (32), 8739−8744.
(33) Kim, H. C.; Suresh, M. V.; Singh, V. V.; Arick, D. Q.; Machado-Aranda, D. A.; Raghavendran, K.; Won, Y.-Y. Polymer Lung Surfactants. *ACS Appl. Bio Mater.* **2018**, *1* (3), 581−592.
(34) Fesenmeier, D. J.; Park, S.; Kim, S.; Won, Y.-Y. Surface mechanical behavior of water-spread poly(styrene)−poly(ethylene glycol) (PS−PEG) micelles at the air−water interface: Effect of micelle size and polymer end/linking group chemistry. *J. Colloid Interface Sci.* **2022**, *617*, 764−777.
(35) Carr, H. Y.; Purcell, E. M. Effects of diffusion on free precession in nuclear magnetic resonance experiments. *Phys. Rev.* **1954**, *94* (3), 630.
(36) Meiboom, S.; Gill, D. Modified spin-echo method for measuring nuclear relaxation times. *Rev. Sci. Instrum.* **1958**, *29* (8), 688−691.
(37) Kim, S.; Park, S.; Fesenmeier, D. J.; Jun, T.; Sarkar, K.; Won, Y.-Y. Surface Pressure−Area Mechanics of Water-Spread Poly(ethylene glycol)-Based Block Copolymer Micelle Monolayers at the Air−Water Interface: Effect of Hydrophobic Block Chemistry. *Langmuir* **2023**, *39* (38), 13546−13559.
(38) Won, Y.-Y.; Paso, K.; Davis, H. T.; Bates, F. S. Comparison of Original and Cross-linked Wormlike Micelles of Poly(ethylene oxide-b-butadiene) in Water: Rheological Properties and Effects of Poly(ethylene oxide) Addition. *J. Phys. Chem. B* **2001**, *105* (35), 8302−8311.
(39) Hrkach, J. S.; Peracchia, M. T.; Bomb, A.; Lotan, n.; Langer, R. Nanotechnology for biomaterials engineering: structural characterization of amphiphilic polymeric nanoparticles by 1H NMR spectroscopy. *Biomaterials* **1997**, *18* (1), 27−30.
(40) Won, Y.-Y.; Davis, H. T.; Bates, F. S.; Agamalian, M.; Wignall, G. D. Segment Distribution of the Micellar Brushes of Poly(ethylene oxide) via Small-Angle Neutron Scattering. *J. Phys. Chem. B* **2000**, *104* (30), 7134−7143.
(41) Johnston, D. C. Stretched exponential relaxation arising from a continuous sum of exponential decays. *Phys. Rev. B* **2006**, *74* (18), No. 184430.
(42) Wu, S. Calculation of interfacial tension in polymer systems. *J. Polym. Sci., Part C: Polym. Symp.* **1971**, *34* (1), 19−30.
(43) Brandrup, J.; Immergut, E. H. *Polymer Handbook*, 3rd ed.; Wiley: New York, 1989.
(44) Wu, S. *Polymer Interface and Adhesion*; Routledge, 2017.
(45) Larison, T.; Stefik, M. Persistent Micelle Corona Chemistry Enables Constant Micelle Core Size with Independent Control of

Functionality and Polyelectrolyte Response. *Langmuir* **2021**, *37* (32), 9817−9825.
(46) Fox, T. G.; Flory, P. J. The glass temperature and related properties of polystyrene. Influence of molecular weight. *J. Polym. Sci.* **1954**, *14* (75), 315−319.
(47) Kim, S.; Lee, M.; Kim, H. C.; Kim, Y.; Lee, W. B.; Won, Y.-Y. Determination of Glass Transition Temperatures in Bulk and Micellar Nanoconfined Polymers Using Fluorescent Molecular Rotors as Probes for Changes in Free Volume. *Macromolecules* **2023**, *56* (16), 6290−6304.

NOTE ADDED AFTER ASAP PUBLICATION

This paper was published ASAP on November 9, 2023, with errors in Figures 2 and 4. The corrected version was reposted on November 10, 2023.

https://doi.org/10.1021/acs.macromol.3c01486
Macromolecules 2023, 56, 9156−9163